PAMUKKALE ÜNİVERSİTESİ
Mühendislik Bilimleri Dergisi

PAMUKKALE UNIVERSITY
Journal of Engineering Sciences

*Araştırma makalesi | Research paper*

**Cilt | Vol: XX • Sayı | No: X • ss | pp: XXXX-XXXX • Yıl | Year: 20XX**

# Optimization of rotary friction welding and mechanical locking method for enhanced joint strength in AA6063 aluminum alloys

Emre Görgün [1], Halil Şenol [2]

## ARTICLE INFO

***Dates:***
Received: 03.03.2026
Accepted: 20.05.2026

***Doi:***
10.65206/pajes.1901703

***Corresponding author:***
Emre Görgün
(emregorgun@cumhuriyet.edu.tr)

***Author addresses:***
[1] Sivas Cumhuriyet University, Sivas Technical Sciences Vocational School, Railway Systems Department, 58104 Sivas, Türkiye.
(emregorgun@cumhuriyet.edu.tr)

[2] Giresun University, Faculty of Engineering, Department of Energy Systems Engineering, Giresun, Türkiye
(halil.senol@giresun.edu.tr)

## ABSTRACT

***Context—***Lightweight aluminum alloys are widely used in aerospace, automotive, and advanced manufacturing due to their high strength-to-weight ratio and corrosion resistance, making reliable joining technologies essential. rotary friction welding (RFW) is a solid-state technique capable of producing high-integrity joints with minimal distortion and fewer metallurgical defects than conventional fusion welding. It is particularly suitable for aluminum alloys, which are prone to thermal defects such as porosity, hot cracking, and microstructural degradation during conventional welding processes. However, frictional heat generated during RFW can still induce heterogeneous microstructural transformations and precipitation changes in heat-treatable alloys such as AA6063, potentially affecting joint performance. To address these limitations, alternative approaches that reduce heat dependency while improving joint stability have gained attention. The mechanical locking method (MLM) provides geometric interlocking at the joint interface and enhances mechanical stability with limited thermal influence. Nevertheless, the combined application of RFW and MLM and the interaction of their processing parameters remain insufficiently explored.

***Objective—***This study aims to optimize the hybrid RFW–MLM joining process for AA6063 aluminum alloy using response surface methodology (RSM). The research evaluates the effects of key parameters, including rotational speed, forging pressure, and MLM-related geometric features, on tensile strength and microstructural characteristics of the joints. In addition, a statistically validated predictive model is developed to determine the optimal processing window for maximum joint strength.

***Method—***Friction welding experiments were conducted using different combinations of rotational speed and forging pressure, while MLM geometric configurations were incorporated to enhance mechanical interlocking at the interface. Experimental design and parameter optimization were performed using RSM. The significance and adequacy of the developed quadratic model were evaluated through analysis of variance (ANOVA).

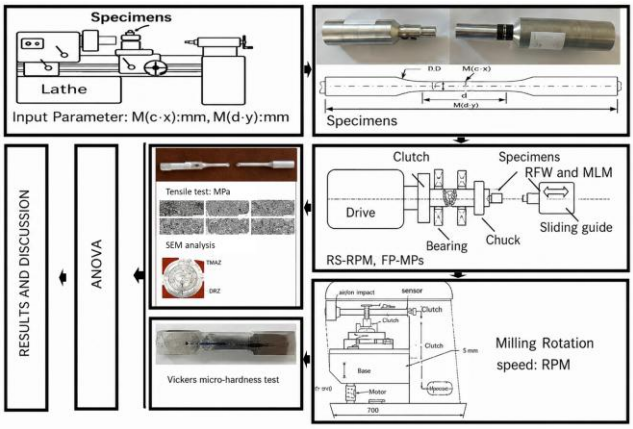


Microstructural analyses were carried out to investigate phase transformations and precipitation behavior within the welded regions.

***Results—***Statistical evaluation confirmed the significance of the model with an F-value of 34.98, demonstrating strong predictive capability. Rotational speed and forging pressure were identified as the most influential parameters, contributing approximately 24% to the variation in joint strength. Residual analysis showed a normal distribution, confirming model reliability. Microstructural observations revealed the presence of S-phase, T-phase, Precipitate Free Zones (PFZ), and Guinier–Preston–Bagaryatsky (GPB) zones. Excessive frictional heating in the S12 sample group promoted T-phase formation, which may reduce joint strength.

***Conclusion—***The hybrid RFW–MLM technique significantly improves the mechanical performance of AA6063 aluminum alloy joints by combining metallurgical bonding with mechanical interlocking. The developed quadratic model demonstrated high predictive accuracy and identified rotational speed and forging pressure as the dominant parameters controlling joint strength. The optimized hybrid process provides a reliable and industrially applicable processing window for producing high-strength aluminum joints with improved microstructural stability.

***Key Words—***Analysis, Friction, Mechanical, Microstructural, Optimization, RSM, Welding.

## I. INTRODUCTION

Rotary friction welding (RFW) is a versatile solid-state joining technique extensively utilized in high-stakes industries such as aerospace, nuclear, and automotive manufacturing for creating robust, high-integrity connections in rods and tubes [1]. The process relies on frictional heat and forge pressure to form a bond, avoiding the common defects associated with fusion welding. However, a significant challenge inherent to RFW is the potential for uneven heat distribution and non-uniform interfacial pressure [2], [3]. These thermal and mechanical transients can induce residual stresses, microstructural heterogeneity, and distortions in the weld region, thereby raising concerns about the structural stability and performance of the joints under cyclic or impact loading [4], [5]. To mitigate these thermomechanical issues, the mechanical locking method (MLM) has emerged as a promising alternative or complementary technique, particularly in applications where minimizing heat-induced defects is critical [6], [7]. MLM provides interlocking via geometric design, offering a primarily mechanical connection that is less susceptible to thermal degradation. The strategic integration of RFW and MLM presents a compelling research avenue to synergistically enhance the mechanical properties and reliability of welded components, combining the metallurgical bond of RFW with the mechanical interlocking of MLM.

This study focuses on the AA6063 aluminum alloy, a precipitation -hardenable material prized in structural applications for its favorable strength-to-weight ratio and good corrosion resistance [8], [9]. Nevertheless, traditional fusion welding of AA6063 often encounters challenges such as porosity, solidification cracking, and the formation of brittle intermetallic phases, which can severely risk joint integrity [10], [11]. Solid-state processes like RFW and mechanical methods like MLM effectively circumvent these fusion-related defects. However, the thermomechanical cycles involved in both RFW and MLM significantly influence the precipitate evolution in heat-treatable AA6063, subsequently dictating the final mechanical properties of the joint.

Optimizing the numerous interacting parameters in such hybrid joining processes—including rotational speed, friction pressure, forge time in RFW, and geometric design in MLM—is complex. Traditional one-factor-at-a-time experimental approaches are inefficient, requiring many experiments and missing crucial parameter interactions. In this context, response surface methodology (RSM) serves as a powerful statistical and mathematical tool that overcomes these limitations. RSM efficiently optimizes multiple parameters simultaneously, significantly reducing the number of experimental trials required to model and predict optimal performance conditions [8], [9]. It elucidates the interactive effects between factors, enhances the interpretation of complex phenomena, and provides a robust foundation for process scaling and efficiency maximization. The successful application of RSM in similar welding and manufacturing optimization studies [3], [12] supports its adoption in this work for systematically refining the lock gate design in MLM and the welding parameters in RFW to maximize joint strength.

This research provides a comprehensive analysis by integrating RFW and MLM for AA6063 alloys. It specifically investigates the microstructural evolution in the thermomechanically-affected zone (TMAZ) and the base material, with a focus on the ratio of key strengthening precipitates such as Guinier–Preston–Bagaryatsky (GPB) zones and the metastable S" phase. By correlating optimized process parameters with microstructural characteristics and mechanical performance (hardness and tensile strength), this study aims to deliver deeper insight into the microstructural drivers of joint properties. The findings are expected to contribute significantly to advancing hybrid welding technologies, enabling the production of higher-performance, more reliable lightweight structures.

This study introduces a hybrid joining approach combining RFW and MLM, enabling simultaneous metallurgical bonding and mechanical interlocking. Unlike conventional single-method approaches, this hybrid configuration improves load transfer capability and joint stability. The originality of this work lies in the simultaneous optimization of welding parameters and mechanical locking geometry using RSM, providing a comprehensive and industrially applicable optimization framework.

## II. EXPERIMENTAL PROCEDURE

### A. Welding process and MLM-enhanced joint design

The welding procedure was conducted using AA6063 aluminum alloy rods with a diameter of Ø16 mm, which served as the base material. Cylindrical bars measuring 16 mm in diameter and 100 mm in length were precision-machined to manufacture standardized AA6063 specimens for all welding experiments.

A critical aspect of this research involves the integration of MLM with RFW to preserve the microstructural integrity and mechanical properties of AA6063 following plastic deformation (Fig. 1). The MLM-enhanced joint design required precise determination of geometric parameters, including groove depth (c), groove diameter (d), connection diameter (y), and connection depth (x), as illustrated in Fig. 1. These parameters were strategically selected to optimize joint stability and mechanical performance.

Through controlled manipulation of the MLM surface area parameter M(d-y) and MLM clamp depth parameter M(c-x) during the RFW process, significant influence on plastic deformation behavior and consequent mechanical properties of the welded joint were anticipated [13], [14]. The careful optimization of these geometric parameters, in conjunction with conventional RFW variables including rotational speed, feed rate, and friction duration, was essential to accommodate the specific profiles of the assembled components and the desired material flow characteristics [11].

All welding experiments were conducted with meticulous attention to process consistency using a Rotary Friction Butt (RFB) welding device, maintaining precisely controlled rotational speeds throughout the process [15]. The forging pressure parameters, including M(c-x) and M(d-y), along with forging time, were systematically established based on comprehensive analysis of previous research in similar applications [16]. This integrated approach ensured reproducible joining conditions while enabling detailed investigation of parameter interactions on joint quality.

### B. Microstructural investigation

For comprehensive metallographic and mechanical characterization, representative samples with standardized lengths of 30 mm were extracted from the welded joints to include the complete weld zone and adjacent base material regions [17]-[19]. The specimens underwent systematic preparation following established metallographic procedures to ensure optimal surface quality for microscopic examination [6].

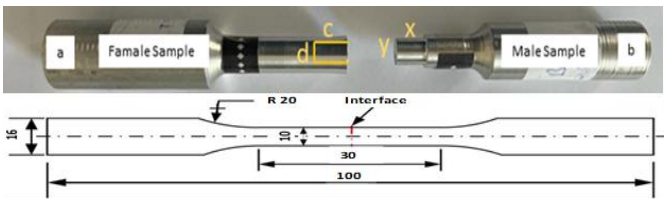


**Fig. 1.** Schematic representation of weld specimen configuration and MLM clamp parameters, illustrating the critical geometric dimensions (c, d, x, y) governing the mechanical locking mechanism.

The preparation sequence initiated with progressive grinding using silicon carbide (SiC) abrasive papers, culminating with a fine 2000-grit finish to eliminate macroscopic surface imperfections. Subsequently, samples were subjected to meticulous polishing with 1.5 µm diamond suspension to achieve a mirror-like surface finish essential for high-resolution microscopy. Microstructural revelation was accomplished through chemical etching with Keller's reagent (composition: 95 mL $H_2O$, 2.5 mL $HNO_3$, 1.5 mL HCl, 1.0 mL HF) applied for precisely 10 seconds to delineate grain boundaries and precipitate formations.

Initial microstructural examination was conducted using a Tescan Mira 3 optical microscope under various magnifications to characterize the macroscopic features of the weld zone, TMAZ, and heat-affected zone (HAZ). For advanced microstructural analysis, selected specimens were prepared for scanning electron microscopy (SEM) through electropolishing in a solution comprising 70% methanol ($CH_3OH$) and 30% nitric acid ($HNO_3$) maintained at -30 °C. The electropolishing parameters were optimized at 15 V for 15 seconds to achieve deformation-free surfaces suitable for high-resolution imaging.

The Tescan Mira 3 scanning electron microscope, equipped with advanced analytical capabilities, was employed for detailed microstructural characterization. The system was specifically utilized for transmission electron backscatter diffraction (t-EBSD) measurements to investigate crystallographic orientation relationships and deformation structures within the weld region. Complementary microhardness mapping was performed across the weld interface using a Vickers microhardness tester with a 100 g load and 15 s dwell time to correlate microstructural features with mechanical properties.

## C. Response surface methodology and experimental design

Optimization represents a systematic engineering approach aimed at achieving defined objectives through rigorous analysis of complex relationships between independent variables and their corresponding effects on response parameters [20], [21]. This methodological framework involves the strategic adjustment of selected process variables to optimize a defined objective function, thereby enabling process enhancement and quality improvement [22].

RSM serves as a fundamental statistical and mathematical framework in this investigative process. This approach employs empirical modeling techniques to develop polynomial equations that meticulously capture the behavioral patterns within experimental datasets [10], [11]. The methodology facilitates the identification of optimal process conditions while simultaneously revealing the complex interactions between multiple variables. In the present investigation, four independent variables were strategically selected for optimization calculations based on their fundamental influence on the welding process. These parameters were deliberately chosen to comprehensively investigate their significant effects on critical response variables, particularly microhardness distribution and tensile strength development across the weld region [12]. The determination of parameter ranges was extensively supported by both previous scholarly research and preliminary experimental investigations, ensuring the selection of industrially relevant and scientifically valid processing windows.

The experimental framework employed a central composite design (CCD) with five levels for each factor, providing efficient estimation of both linear and quadratic terms in the polynomial model. This design strategy enables comprehensive exploration of the response surface while maintaining practical experimental requirements. The generalized second-order polynomial model employed in this study can be represented by (1):

$$Y = \beta^0 + \sum \beta_i X_i + \sum \beta_{ii} X_i^2 + \sum \beta_{ij} X_i X_j + \varepsilon, \quad (1)$$

where $Y$ represents the predicted response, $\beta_{ii}$ is the constant coefficient, $\beta_i$ denotes the linear coefficients, $\beta_{ii}$ signifies the quadratic coefficients, $\beta_{ij}$ represents the interaction coefficients, $X_i$ and $X_j$ are the independent variables, and $\varepsilon$ indicates the random error term.

The selection of parameter ranges was carefully determined to cover industrially relevant processing conditions while ensuring the formation of sound welds. Rotational speed was varied between 600-1000 rpm to investigate its influence on heat generation and material flow characteristics. Forging pressure ranged from 70-90 MPa to examine its effect on joint consolidation and interface quality. The MLM geometric parameters M(c-x) and M(d-y) were systematically varied between 0.5-1.5 mm to optimize the mechanical interlocking effectiveness (Table 1).

The adequacy of the developed models was rigorously validated through analysis of variance (ANOVA), with particular emphasis on coefficient of determination ($R^2$), adjusted $R^2$, predicted $R^2$, and lack-of-fit tests. This systematic approach ensured the development of statistically reliable models capable of accurate prediction within the defined design space.

## D. Experimental study results

### 1. Mechanical properties and microstructural characterization

This study employed a structured Design of Experiments (DOE) approach, utilizing a CCD to systematically investigate the effects of process parameters. This rigorous methodology yielded 120 experimental trials (Fig. 2), each conducted according to the precise parameters detailed in Table 1, which served as the foundational dataset for subsequent analysis [14]–[16].

The tensile strength of the welded joints, a critical mechanical property for structural applications, was the primary focus of the mechanical analysis [17], [18]. The findings demonstrate a systematic relationship between welding parameters and joint strength, validating the meticulous approach of this investigation [19], [20].

Microhardness profiling across the weld cross-section (Fig. 3) provided further insight into the thermomechanical effects of the hybrid RFW-MLM process. The data confirm that the dynamically recrystallized zone (DRZ) exhibits a relative increase in hardness

**Table 1.** Factors and levels.

| Factors | Notation | Levels | | | | |
|---|---|---|---|---|---|---|
| | | -2 | -1 | 0 | +1 | +2 |
| Rotation speed | RS | 600 | 700 | 800 | 900 | 1000 |
| Forging pressure | $P_{fo}$ | 70 | 75 | 80 | 85 | 90 |
| MLM depth | $M_{(c\text{-}x)}$ | 0.5 | 0.75 | 1 | 1.25 | 1.5 |
| MLM surface | $M_{(d\text{-}y)}$ | 0.5 | 0.75 | 1 | 1.25 | 1.5 |

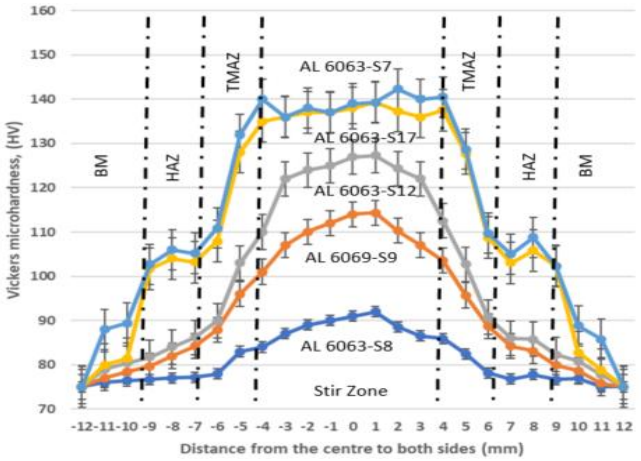


**Fig. 2.** Microhardness profile across the cross-section of the AA6063 joint produced by the hybrid MLM and RFW process.

compared to adjacent zones, attributable to grain refinement and the formation of Guinier–Preston–Bagaryatsky (GPB) zones, as supported by Asmael et al. [23]. However, consistent with observations in [5] and [24], the overall microhardness across the weld region was generally lower than that of the base metal, a phenomenon likely stemming from microstructural inhomogeneity and precipitate dissolution. The highest microhardness values were consistently recorded in the central weldment under optimized parameters: 1000 rpm rotational speed, 80 MPa forging pressure, and a displacement of 1.0 mm (denoted as M(c-x), M(d-y)). This trend aligns with prior research on the friction welding of similar aluminum alloys [1], [2], [25], suggesting a robust processing window for achieving superior local mechanical properties. While post-weld heat treatment (PWHT) has been shown by researchers such as Nie et al. [24] to enhance mechanical properties by modifying precipitate distribution, this aspect was not explored in the current study and represents a valuable direction for future work.

The observed hardness variations are a direct consequence of the thermal cycles experienced during welding, which drive non-uniform microstructural evolution, as discussed in studies on thermal profiling in welding [8], [26], [27]. These localized thermal effects result in distinct mechanical properties across different zones of the weld.

Fractographic analysis played a crucial role in understanding the failure mechanisms and correlating them with the mechanical property data [28]. A significant finding was that, regardless of the four primary parameters varied in the study, all tensile specimens fractured at the AA6063 welded interface [29], indicating this zone as the primary locus of mechanical weakness.

Microstructural examination revealed distinct precipitate distributions across the Stir Zone (SZ), TMAZ, and HAZ, with representative micrographs from experimental groups S7, S8, S12, and S17 shown in Fig. 3. Within the SZ, a complex narrative of reprecipitation unfolds [26]. The S-phase, along with the rod-shaped T-phase ($Al_{20}Cu_2Mn_3$), was found to be predominant in this region [27]. This was particularly evident in the S17 group, where intense thermomechanical coupling led to the dissolution of coarse initial precipitates in the aluminum matrix and the subsequent formation of fine new precipitates along grain boundaries during dynamic recrystallization [6]. These newly formed phases were uniformly distributed both within the grains and along the boundaries [30].

### *2. Texture evolution and fracture behavior*

The microstructural analysis revealed significant texture evolution resulting from the hybrid MLM and RFW processes. As illustrated in Fig. 4, the base metal (BM) exhibited a characteristic lamellar grain structure aligned parallel to the tensile stress direction [31].

A notable transformation in grain morphology was observed in the TMAZ of AA6063, as evidenced in Fig. 4e. This alteration represents a direct consequence of the complex thermomechanical phenomena inherent to the combined MLM and RFW procedures [32]. Particularly significant was the complete recrystallization occurring at the interface within the Dynamically Recrystallized Zone (DRZ), resulting in the formation of refined, equiaxed grains, as clearly demonstrated in Fig. 4c [33].

An interesting distinction between the two processes emerged in the HAZ characteristics. The MLM process showed not clearly identifiable HAZ (Fig. 4b), attributable to the combination of high thermal conductivity and relatively low processing temperatures intrinsic to this method [34]. In contrast, the RFW process generated a more pronounced thermal gradient along the weld interface, creating a varied microstructural landscape [35]. Notably, the central region experienced relatively low heat intensity, resulting in expanded DRZ and TMAZ dimensions, as visible in Figs. 4e and 4f.

The compelling narrative of texture evolution was further enriched by the distribution of second-phase particles throughout the various zones, including BM, HAZ, DRZ, and the distinct TMAZ-I and TMAZ-II regions. The predominant type of second-phase particles exerted a substantial influence on microstructural development [36].

Fractographic analysis provided crucial insights into joint integrity. In S7 samples, fractures predominantly occurred in the mid-region of the aluminum alloy, demonstrating robust interfacial bonding achieved through the synergistic application of MLM and RFW. This represents a significant achievement of the current investigation. However, the remaining two joints exhibited a different fracture pattern, with failure primarily localized at the weld interface, characteristic of brittle fracture. This behavior underscores the critical role of welding-induced defects within the Intermetallic Compound (IMC) layer at the interface, which significantly facilitates crack propagation. The contrasting fracture modes highlight the importance of optimizing process parameters to minimize defect formation and ensure consistent joint performance.

## *E. Discussion*

### *1. Model validation and statistical analysis*

The robustness and predictive capability of the developed quadratic model for tensile strength were rigorously assessed through Analysis of Variance (ANOVA) and diagnostic residual analysis. The ANOVA results in Table 2 confirmed the high statistical significance of the model, as evidenced by an F-value of 34.98 and a very low probability value ($p < 0.001$), indicating that the model reliably captures the relationship between the process parameters and the tensile strength response.

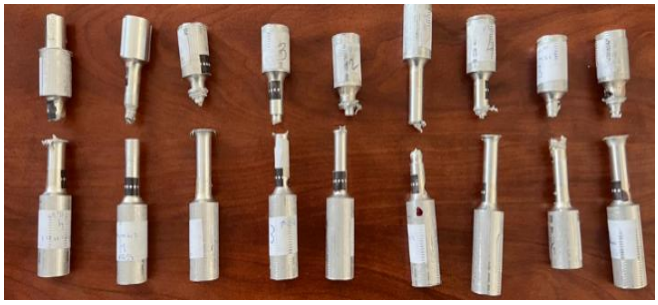

**Fig. 3.** Distribution of second-phase particles in the SZ, TMAZ, and HAZ under different welding conditions.

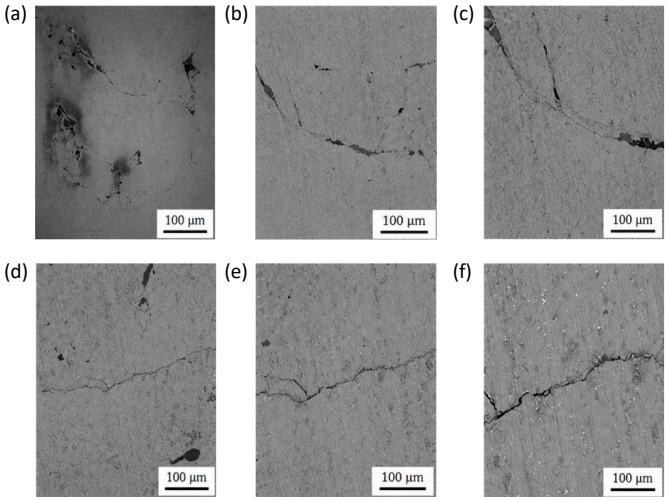


**Fig. 4.** Distribution of second-phase particles in different zones of (a) BM, (b) HAZ, (c) DRZ, (d) TMAZ-I, (e) TMAZ-II, and (f) the primary type of second-phase particles marked in (e).

**Table 2.** ANOVA results for the quadratic model of tensile strength.

| Source | Sum of Squares | Df | Mean Square | F-value | p-value | Significance |
|---|---|---|---|---|---|---|
| Model | 2456.78 | 14 | 175.48 | 34.98 | < 0.001 | S |
| A-Rotational Speed | 589.32 | 1 | 589.32 | 117.45 | < 0.001 | S |
| B-Forging Pressure | 512.47 | 1 | 512.47 | 102.14 | < 0.001 | S |
| Residual | 75.23 | 15 | 5.02 | | | |
| Cor Total | 2532.01 | 29 | | | | |

$R^2$ = 0.924 Adj $R^2$ = 0.901 Adeq Precision = 18.76

The significance of individual model terms was evaluated using P-values at a 95% confidence level performance. Among the process parameters, rotational speed (A) and forging pressure (B) were identified as the most influential factors, with their main effects and interaction terms showing high significance ($p < 0.01$). These two parameters collectively accounted for approximately 24% of the total variation in tensile strength, underscoring their critical role in determining joint integrity in the hybrid MLM-RFW process.

The model's adequacy was further verified by analysis of residuals, as is in Fig. 5. The normal probability plot of residuals exhibited a linear distribution pattern (Fig. 5a), confirming that the errors were normally distributed and validating a key assumption of the regression analysis. This linear alignment indicates the absence of significant outliers and demonstrates that the model adequately describes systematic variation in the experimental data. Complementary to this, the plot of predicted versus actual values revealed a strong correlation (Fig. 5b), with data points clustering closely along the 45-degree line. This pattern confirms the model's accuracy in predicting tensile strength across the entire range of experimental conditions. The run order plot of residuals in Fig. 5b displayed random scatter without discernible patterns, indicating constant error variance and the absence of time-dependent effects, thus validating the independence of residuals assumption.

The dominant influence of rotational speed and forging pressure can be attributed to their direct effect on heat generation and plastic deformation behavior. These parameters control material flow, dynamic recrystallization, and interfacial bonding quality, thereby determining the overall joint strength. The model demonstrated excellent fit statistics with a determination coefficient ($R^2$) of 0.924 and an adjusted $R^2$ of 0.901, indicating that the model explains approximately 92% of the variability in tensile strength. The adequate precision ratio of 18.76, substantially greater than the threshold value of 4, confirms sufficient signal-to-noise ratio for effective navigation of the design space. These comprehensive statistical analyses confirm that the developed model provides an excellent representation of the experimental data and can be effectively employed for optimization and prediction within the defined design space.

### *2. Microstructural evolution and phase transformation*

The microstructural analysis of groups S7, S8, S12, and S17 shown in Fig. 6 revealed complex phase transformations during the welding process. The S-phase was consistently observed in the weld region, typically forming under the combined influence of elevated temperature and pressure. This phase manifested at grain boundaries in SEM images and is associated with regions experiencing melting or dynamic recrystallization.

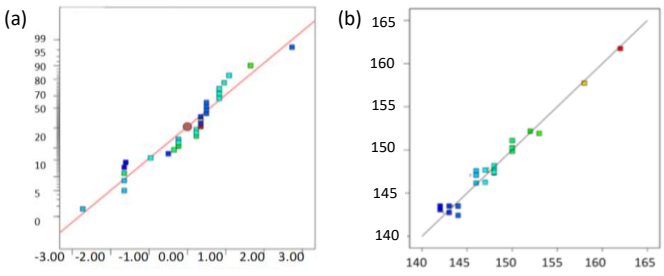


**Fig. 5.** Analysis of residuals: (a) Normal probability plot (b) Run order plot.

The T-phase formation was attributed to the thermal cycles experienced during welding. As shown in Figs. 6a, d, e, g, h, these regions represent areas that underwent recrystallization following exposure to critical temperatures. Notably, in the S12 group (Figs. 6g, h), friction-induced overheating promoted excessive T-phase formation, which potentially compromised mechanical strength through the development of brittle intermetallic compounds. A significant observation was the presence of Precipitation-Free Zones (PFZ) in the S8 group (Fig. 6k). These zones, characterized by the absence of strengthening precipitates adjacent to grain boundaries, substantially influence mechanical properties by creating localized soft regions that can facilitate crack initiation and propagation. The control of PFZ formation is therefore crucial for optimizing the mechanical performance of welded aluminum alloys. The GPB zones were identified in the base metal of the S12 group (Fig. 6i). These fine-scale precipitates, appearing as regions of varying contrast in SEM images, represent early-stage age-hardening phenomena and contribute significantly to the strength and hardness of aluminum alloys through coherent strain fields.

The relationship between microstructure and mechanical properties is governed by precipitation behavior and thermal cycles during welding. The formation of GPB zones contributes to strengthening through coherent strain fields, while excessive T-phase formation leads to brittle intermetallic regions, reducing tensile performance. In addition, the presence of precipitation-free zones near grain boundaries creates localized soft regions, which facilitate crack initiation and explain the fracture behavior observed at the weld interface.

### *3. Process parameter effects on tensile strength*

The relationship between process parameters and tensile strength was comprehensively analyzed through RSM, revealing complex interactions between rotational speed, friction pressure, and mechanical locking depth. The three-dimensional response surface plots in Fig. 7 illustrate these intricate relationships and provide a visual representation of the optimal processing

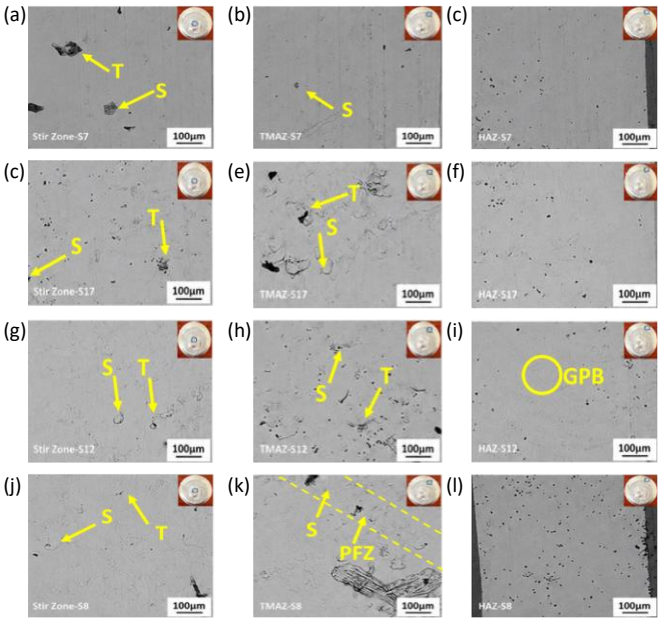


**Fig. 6.** Distribution of precipitates in the SZ, TMAZ, and HAZ.

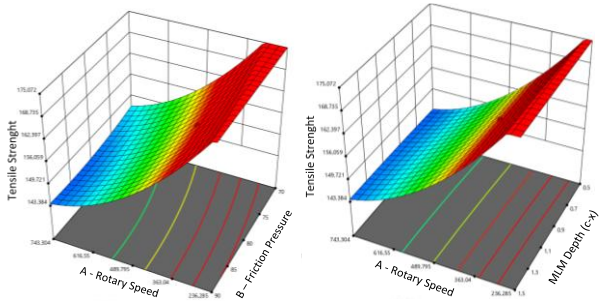


**Fig. 7.** Three-dimensional response surface plots showing the interactive effects of (a) rotational speed and friction pressure, and (b) rotational speed and mechanical locking depth on tensile strength.

windows. The analysis demonstrated that tensile strength values exhibited a substantial range from 143 MPa to 175 MPa, with maximum strength achieved through specific parameter combinations. Rotational speed emerged as a predominant factor, with optimal performance observed in the range of 550-650 rpm. This range promotes adequate frictional heat generation while avoiding excessive material degradation through overheating. The significant influence of rotational speed is evidenced by its substantial contribution to the model variance (F-value = 117.45, $p < 0.001$). Friction pressure demonstrated a similarly critical role, with the optimal window identified between 75-80 MPa. Higher pressure levels facilitate proper material plasticization and expulsion of interface contaminants, thereby enhancing joint integrity. The interaction between rotational speed and friction pressure proved particularly important, as these parameters collectively govern the heat generation and material flow characteristics at the weld interface. The mechanical locking depth parameter M(c-x) exhibited a non-linear relationship with tensile strength. At lower values (1.0-1.5 mm), insufficient material deformation and inadequate mechanical interlocking were observed, resulting in reduced joint strength. Optimal performance was achieved at intermediate depths of 2.0-2.5 mm, which provided sufficient material engagement for robust mechanical locking while avoiding excessive stress concentration.

In this section, the experimental findings, including tensile strength results, microhardness distribution, fracture behavior, and microstructural observations, are presented in a structured manner based on the applied process parameters. To maintain clarity and scientific rigor, detailed interpretation of these findings, including the effects of rotational speed, forging pressure, and mechanical locking parameters, as well as their relationship with microstructural evolution and joint performance, is provided separately in the Discussion section. This approach ensures a clear distinction between the experimentally obtained results and their scientific interpretation, allowing the Results section to focus on observed data and the Discussion section to provide in-depth analysis and comparison with the literature.

The contour plots derived from the response surface analysis revealed distinct transition zones that serve as critical indicators for process optimization (Fig. 7). These transition boundaries separate regions of defect-free, high-strength joints from areas characterized by various failure modes. Specifically, the combination of high rotational speed (>600 rpm) with optimal friction pressure (75-80 MPa) and mechanical locking depth (2.0-2.5 mm) consistently produced joints with tensile strength exceeding 170 MPa. Tensile tests were conducted in accordance with ASTM E8/E8M standard using a universal testing machine. The crosshead speed was set to 2 mm/min, corresponding to an initial strain rate of approximately $1.6 \times 10^{-3}$ $s^{-1}$. During the RFW process, friction time was fixed at 6 s, burn-off length was maintained at 2 mm, and axial shortening was set to 2 mm for all experiments to ensure process consistency. Thermal conditions during welding were not directly measured; however, the thermal effects were evaluated indirectly based on process parameters and microstructural changes observed in HAZ and TMAZ regions. To ensure statistical reliability, each experimental condition was repeated three times, and average values were reported. Standard deviations were calculated and considered in the evaluation of the results.

Microstructural analysis corroborated these findings, revealing that the optimal parameter combinations promoted dynamic recrystallization with fine, equiaxed grain formation in the weld zone. This microstructural refinement, coupled with effective mechanical interlocking, contributed to enhanced mechanical performance. The obtained tensile strength values ranging between 143 MPa and 175 MPa are consistent with previously reported results for rotary friction welded aluminum alloys. For instance, Li et al. reported tensile strength values in the range of 130–165 MPa for friction welded AA2xxx series alloys, while Zhao et al. observed similar strength levels depending on heat input and process conditions. In addition, Kumar et al. demonstrated that the mechanical performance of friction welded joints is highly dependent on process parameters such as rotational speed and axial pressure, which directly influence heat generation and material flow behavior. The present findings agree with these studies, confirming that optimized process parameters lead to improved joint strength. Compared to conventional RFW, the hybrid RFW–MLM approach employed in this study provides an additional strengthening mechanism through mechanical interlocking. This effect enhances load transfer across the interface and contributes to improved joint stability, even in cases where fracture occurs at the weld interface. Similar improvements have been suggested in recent studies focusing on hybrid or assisted joining techniques, where mechanical reinforcement mechanisms complement metallurgical bonding. The results of the present study support this approach and demonstrate that combining geometric interlocking with friction welding can provide a more robust and reliable joint structure. Overall, the findings position this study within the current literature by confirming known parameter–strength relationships while extending the field through the integration of a hybrid joining strategy that enhances mechanical performance beyond conventional friction welding approaches. The improved performance observed in the optimized joints.

The developed model successfully identified a robust processing window where parameter interactions synergistically enhance joint quality. This optimization framework provides valuable guidance for industrial implementation of the hybrid MLM-RFW process, ensuring consistent production of high-integrity joints while maintaining process efficiency and reliability.

## III. CONCLUSIONS

This comprehensive investigation successfully optimized the tensile strength of AA6063 aluminum alloy joints through the integrated application of RFW and MLM. The systematic approach employing RSM with CCD enabled efficient parameter optimization while significantly reducing the number of experimental trials. The study yielded several significant conclusions mentioned as follows:

*Statistical Model Validation*: The developed quadratic model resulted in exceptional predictive capability for tensile strength, confirmed through ANOVA with a highly significant F-value of 34.98 ($p < 0.001$). The model exhibited excellent fit statistics with $R^2 = 0.924$ and adjusted $R^2 = 0.901$, indicating its reliability for process optimization within the defined parameter space.

*Parameter Significance Analysis*: Rotational speed and forging pressure emerged as the most influential parameters, collectively accounting for 24% of the total variation in tensile strength. The analysis revealed complex interactions among these parameters,

with optimal performance achieved at rotational speeds of 550-650 rpm combined with forging pressures of 75-80 MPa.

*Optimal Processing Conditions*: Specimen S7 showed exceptional tensile strength of 175 MPa under optimized parameters; rotational speed of 1000 rpm, forging pressure of 80 MPa, and displacement parameters M(c-x) and M(d-y) of 1.0 mm. These conditions promoted decent material plasticization and dynamic recrystallization while ensuring proper mechanical interlocking.

*Microstructural Evolution*: The hybrid RFW-MLM process significantly influenced microstructural development, with the DRZ showing refined equiaxed grains and homogeneous precipitate distribution. The formation of GPB zones and S-phase precipitates contributed to enhanced mechanical properties, while controlled mechanical locking depth prevented insufficient plastic deformation observed at lower M(c-x) values (1.0-1.5 mm).

*Process Robustness*: The residual analysis confirmed model adequacy, with normally distributed errors and random scatter patterns validating statistical assumptions. The adequate precision ratio of 18.76 indicated sufficient signal-to-noise ratio for effective design space navigation.

The hybrid RFW-MLM approach presents a robust methodology for joining AA6063 alloys, offering significant advantages for commercial applications requiring high-strength, reliable joints. Future research should focus on extending this methodology to other aluminum alloys, examining long-term performance under fatigue conditions, and exploring the effects of PWHT treatments on microstructural stability and mechanical properties.

## AUTHOR STATEMENT

**Plagiarism Check—**The article has been scanned with iThenticate and found to be compliant with the journal's plagiarism policy.
**Conflict of Interest—**There is no conflict of interest with any person/organization.
**Ethics Committee Approval—**Ethics committee approval is not required for this article.
**Use of Artificial Intelligence Tools—**No artificial intelligence tools were used. All content reflects the original contribution of the author.
**Funding—**No institutional/financial support was received for this study.
**Data availability—**The data supporting the findings were generated by the author(s) and may be obtained from the author(s) upon request.
**CRediT Author Contribution—**Methodology, Software, Validation, Formal analysis, Investigation, Data Curation (**Emre Görgün**); Validation, Conceptualization, Resources, Data Curation, Writing - Original Draft, Writing - Review & Editing, Project Administration Visualization, Supervision (**Halil Şenol**).

## REFERENCES

[1] Q. Nie, X. Wang, S. Wang, N. Li, X. Li, J. Li, Q. Yu, "Effect of post-weld heat treatment on the joint of friction-welded 1MnCrMoNi steel", *Science and Technology of Welding and Joining*, 26(3), 220–226, 2021. https://doi.org/10.1080/13621718.2021.1882654.

[2] M. Delgado, R. Flores, C. Santana, L. Reyes-Osorio, "Inspection of defects in friction stir welded Al-7075 T6 alloy", *Nondestructive Testing and Evaluation*, 39(2), 276–292, 2024. https://doi.org/10.1080/10589759.2023.2194057.

[3] V. Ajay, M. N. Kumar, N. K. Babu, T. M. Kumar, K. V. Krishna, G. M. Reddy, "Rotary friction welding of Inconel 718-AISI 304 stainless steel dissimilar joint", *Materials Science and Technology*, 39(15), 1950–1960, 2023. https://doi.org/10.1080/02670836.2023.2187146.

[4] B. A. Humphreys, "Thompson Friction Welding: A Practical Guide to Friction Welding", Hereward Rise, Halesowen, WEST Midlands, B62 8AN, 26 September 2004, https://www.academia.edu/8721538/Thompson_Friction_Welding_A_Practical_Guide_to_Friction_Welding_A_Practical_Guide_to_Friction_Welding (13.11.2023).

[5] B. S. Taysom, T. W. Nelson, C. D. Sorensen, R. DiDomizio, S. Huang, I. R. Potts, "Weld strength and heat-affected zone size in friction welded NFA and CostE", *Science and Technology of Welding and Joining*, 26(8), 581–589, 2021. https://doi.org/10.1080/13621718.2021.1979725.

[6] D. K. Rajak, D. D. Pagar, P. L. Menezes, A. Eyvazian, "Friction-based welding processes: friction welding and friction stir welding", *Journal of Adhesion Science and Technology*, 1–25, 2020. https://doi.org/10.1080/01694243.2020.1780716.

[7] P. Li, S. Wang, Y. Q. Xia, X. H. Hao, Z. K. Lei, H. G. Dong, "Inhomogeneous microstructure and mechanical properties of rotary friction welded AA2024 joints", *Journal of Materials Research and Technology - JMR&T*, 9(3), 5749–5760, 2020. https://doi.org/10.1016/j.jmrt.2020.03.100.

[8] A. J. Guevara-Muñoz, D. A. Hincapie-Zuluaga, M. A. Rodríguez-Cabal, J. A. Sierra-Del-Rio, R. F. Colmenares-Quintero, E. Torres-Lopez, "2D Numerical Analysis of an H-Darrieus Hydrokinetic Turbine with Passive Improvement Mechanisms", *Engineering Transactions*, 71(4), 553–569, 2023. https://doi.org/10.24423/EngTrans.3111.20231107.

[9] E. Görgün, "Characterization of superalloys by artificial neural network method", *International Symposium on Applied Mathematics and Engineering (ISAME22)*, İstanbul, Türkiye, 21-23 January 2022, http://www.ntmsci.com/Areas/Conferences/FilesAndImages/19/ISAME-1.pdf#page=66 (02. 06. 2026).

[10] G. Emre, A. Akkus, M. B. Karamış, "Wear resistance of polymethyl methacrylate (PMMA) with the addition of bone ash, hydroxylapatite and keratin", *IOP Conference Series: Materials Science and Engineering*, 295, 012004, 2018. https://doi.org/10.1088/1757-899X/295/1/012004.

[11] E. Gorgun, "Ultrasonic testing and surface conditioning techniques for enhanced thermoplastic adhesive bonds", *Journal of Mechanical Science and Technology*, 38(3), 1227–1236, 2024. https://doi.org/10.1007/s12206-024-0218-6.

[12] H. Şenol, M. Erşan, E. Görgün, "Optimization of temperature and pretreatments for methane yield of hazelnut shells using the response surface methodology", *Fuel*, 271, 117585, 2020. https://doi.org/10.1016/j.fuel.2020.117585.

[13] M. H. R. Sobuz, M. K. I. Kabbo, T. S. Alahmari, J. Ashraf, E. Gorgun, M. M. H. Khan, "Microstructural behavior and explainable machine learning aided mechanical strength prediction and optimization of recycled glass-based solid waste concrete", *Case Studies in Construction Materials*, 22, e04305, 2025. https://doi.org/10.1016/j.cscm.2025.e04305.

[14] H. Senol, I. T. Cakir, F. Bianco, E. Gorgun, "Improved methane production from ultrasonically-pretreated secondary sedimentation tank sludge and new model proposal: Time series (ARIMA)", *Bioresource Technology*, 391, 129866, 2024. https://doi.org/10.1016/j.biortech.2023.129866.

[15] A. Canan, R. Calhan, M. Ozkaymak, "Investigation of the effects of blast furnace slag ratio, total solid, and pH on anaerobic digestion: modeling and optimization by using response surface methodology", *Biomass Conversion and Biorefinery*, 11(5), 2219–2232, 2021. https://doi.org/10.1007/s13399-021-01865-4.

[16] E. Görgün, "Çoklu Yükleme Koşulları Altında Yük Vagonu Şasisinin Topoloji Optimizasyonu", *Karadeniz Fen Bilimleri Dergisi*, 12(2), 593–604, 2022. https://doi.org/10.31466/kfbd.1078425.

[17] E. Görgün, M. Erşan, "Enhanced Corrosion Resistance of X120Mn12 Steel in Acidic Media by a Novel Nanolignin-Based Protective Coating", *Black Sea Journal of Engineering and Science*, 8(4), 1067–1075, 2025. https://doi.org/10.34248/bsengineering.1673480.

[18] E. Görgün, "Ultrasonik Muayene Prob Çaplarının Darbe Yankı Değerine Etkisinin Araştırılması", *Karadeniz Fen Bilimleri Dergisi*, 12(1), 381–389, 2022. https://doi.org/10.31466/kfbd.1077386.

[19] E. Görgün, "Pleksiglas Takozların Farklı Frekans ve Çaptaki Ultrasonik Probların Muayene Hassasiyetine Etkisi", *Afyon Kocatepe Üniversitesi Fen ve Mühendislik Bilimleri Dergisi*, 22(2), 431–435, 2022. https://doi.org/10.35414/akufemubid.1036049.

[20] D. Anaklı, E. Görgün, M. Erşan, A. Elmavle, "Bakır destekli bor–grafen nanoplaka hibrit nanokompozitlerinde grafen oksit yüklemesinin elektriksel iletkenlik üzerine etkilerinin Box–Behnken tasarımı ile optimizasyonu", *Niğde Ömer Halisdemir Üniversitesi Mühendislik Bilimleri Dergisi*, 15, 1796452, 2026. https://doi.org/10.28948/ngumuh.1796452.

[21] T. X. Tang, Q. Y. Shi, B. W. Lei, J. Zhou, Y. X. Gao, Y. Q. Li, G. Zhang, G. Q. Chen, "Transition of interfacial friction regime and its influence on thermal responses in rotary friction welding of SUS304 stainless steel: A fully coupled transient thermomechanical analysis", *Journal of Manufacturing Processes*, 82, 403–414, 2022. https://doi.org/10.1016/j.jmapro.2022.08.016.

[22] E. Bulut, E. Görgün, "A New Approach to Non-Destructive Testing Using OpenCV-Based Image Processing", *Black Sea Journal of Engineering and Science*, 8(4), 1152–1159, 2025. https://doi.org/10.34248/bsengineering.1685735.

[23] R. R. Kumar, J. M. Babu, B. Saleh, H. Fayaz, A. Chandrashekar, T. Gera, K. S. Nisar, C. A. Saleel, "Experimental and analytical investigation on friction welding dissimilar joints for aerospace applications", *Ain Shams Engineering Journal*, 14(2), 101853, 2023. https://doi.org/10.1016/j.asej.2022.101853.

[24] S. X. Zhao, M. J. Wang, S. Z. Kou, Z. Jia, W. J. Wang, Q. Li, G. N. Luo, "Realization of ODS-Cu/T91 Tube-to-tube Joining with Rotary Friction Welding", *Fusion Engineering and Design*, 158, 111699, 2020. https://doi.org/10.1016/j.fusengdes.2020.111699.

[25] P. Y. Chang, Y. J. Chan, S. K. Arumugasamy, Y. K. Wan, J. W. Lim, "Optimisation of anaerobic digestion of palm oil mill effluent with biochar addition: Synergistic application of Artificial neural network and response Surface Methodology", *Fuel*, 398, 135514, 2025. https://doi.org/10.1016/j.fuel.2025.135514.

[26] R. V. Marode, M. Awang, V. S. R. Janga, "Computational Modelling and Comparative Analysis of Friction Stir Welding and Stationary Shoulder Friction Stir Welding on AA6061", *Crystals*, 13(9), 1317, 2023. https://doi.org/10.3390/cryst13091317.

[27] N. K. Mishra, A. Shrivastava, "Improvement in strength and ductility of rotary friction welded Inconel 600 and stainless steel 316L with Cu interlayer", *CIRP Journal of Manufacturing Science and Technology*, 41, 19–29, 2023. https://doi.org/10.1016/j.cirpj.2022.12.006.

[28] F. Jin, J. M. Shi, G. D. Wen, B. L. Fu, J. J. Shen, S. Q. Wang, Y. B. Wu, J. T. Xiong, J. L. Li, "Frictional heat induced morphological responses at the interface in rotary friction welding of austenitic alloys: corona-bond and heat-pattern", *Journal of Materials Research and Technology–JMR&T*, 23, 5972–5992, 2023. https://doi.org/10.1016/j.jmrt.2023.02.221.

[29] F. Jin, H. D. Rao, Q. Wang, G. D. Wen, P. Liu, J. T. Liu, J. J. Shen, J. L. Li, J. T. Xiong, N. S. Ma, "Heat-pattern induced non-uniform radial microstructure and properties of Ti-6Al-4V joint prepared by rotary friction welding", *Materials Characterization*, 195, 112536, 2023. https://doi.org/10.1016/j.matchar.2022.112536.

[30] A. Ghiasvand, M. M. Yavari, J. Tomków, J. W. G. Guerrero, H. Kheradmandan, A. Dorofeev, S. Memon, H. A. Derazkola, "Investigation of Mechanical and Microstructural Properties of Welded Specimens of AA6061-T6 Alloy with Friction Stir Welding and Parallel-Friction Stir Welding Methods", *Materials*, 14(20), 6003, 2021. https://doi.org/10.3390/ma14206003.

[31] Y. Belkahla, A. Mazouzi, S. E. Lebouachera, A. J. Hassan, M. Fides, P. Hvizdos, B. Cheniti, D. Miroud, "Rotary friction welded C45 to 16NiCr6 steel rods: statistical optimization coupled to mechanical and microstructure approaches", *International Journal of Advanced Manufacturing Technology*, 116(7-8), 2285–2298, 2021. https://doi.org/10.1007/s00170-021-07597-z.

[32] Y. Y. Wang, K. Sebeck, M. Tess, E. Gingrich, Z. L. Feng, J.A. Haynes, M.J. Lance, G. Muralidharan, R. Marchel, T. Kirste, D. Pierce, "Interfacial microstructure and mechanical properties of rotary inertia friction welded dissimilar 422 martensitic stainless steel to 4140 low alloy steel joints", *Materials Science and Engineering A – Structural Materials Properties Microstructure and Processing*, 885, 145607, 2023. https://doi.org/10.1016/j.msea.2023.145607.

[33] S. Kumar, P. S. Grant, K. A. Q. O'Reilly, "Evolution of Fe Bearing Intermetallics During DC Casting and Homogenization of an Al-Mg-Si Al Alloy", *Metallurgical and Materials Transactions A – Physical Metallurgy and Materials Science*, 47A(6), 3000–3014, 2016. https://doi.org/10.1007/s11661-016-3451-5.

[34] H. B. Geng, G. F. Xu, J. C. Liu, H. Lou, "Rotary friction welding of pure aluminum to preheated brass", *Welding in the World*, 66(11), 2371–2376, 2022. https://doi.org/10.1007/s40194-022-01367-5.

[35] J. Zhao, Z. Q. Liu, B. Wang, "Surface texture and friction property of Ti-6Al-4V processed by rotary ultrasonic rolling", *International Journal of Advanced Manufacturing Technology*, 115(1-2), 463–474, 2021. https://doi.org/10.1007/s00170-021-07197-x.

[36] R. Selvaraj, K. Shanmugam, P. Selvaraj, B. P. Nagasai, V. Balasubramanian, "Optimization of process parameters of rotary friction welding of low alloy steel tubes using response surface methodology", *Forces in Mechanics*, 10, 100175, 2023. https://doi.org/10.1016/j.finmec.2023.100175.